


**Key Points:**

- First time series of Iceland Scotland Overflow Water (ISOW) transport through the Bight Fracture Zone (BFZ) indicates mean of  $-0.6 \pm 0.3$  Sv (westward)
- These year-round observations of ISOW transport through the BFZ reveal, for the first time, wintertime flow reversals and an annual cycle
- Deep floats show a direct advective pathway into the BFZ that appears most influenced by local bathymetry

**Supporting Information:**

Supporting Information may be found in the online version of this article.

**Correspondence to:**

H. Furey,  
hfurey@whoi.edu

**Citation:**

Furey, H., Bower, A., Ramsey, A., Houk, A., & Meunier, T. (2024). Variability of Iceland Scotland Overflow Water across the Reykjanes Ridge: Two-years of moored observations in the Bight Fracture Zone. *Journal of Geophysical Research: Oceans*, 129, e2023JC020463. <https://doi.org/10.1029/2023JC020463>

Received 8 SEP 2023

Accepted 1 MAY 2024




**Author Contributions:**

**Conceptualization:** H. Furey, A. Bower  
**Data curation:** H. Furey, A. Ramsey, A. Houk, T. Meunier  
**Formal analysis:** H. Furey, A. Houk, T. Meunier  
**Funding acquisition:** A. Bower  
**Investigation:** H. Furey, A. Ramsey  
**Methodology:** H. Furey, A. Bower  
**Project administration:** A. Bower  
**Resources:** A. Bower  
**Software:** H. Furey, A. Ramsey, A. Houk, T. Meunier  
**Supervision:** H. Furey, A. Bower  
**Validation:** H. Furey  
**Visualization:** H. Furey, A. Ramsey

© 2024 The Authors.

This is an open access article under the terms of the [Creative Commons Attribution-NonCommercial License](https://creativecommons.org/licenses/by-nc/4.0/), which permits use, distribution and reproduction in any medium, provided the original work is properly cited and is not used for commercial purposes.

# Variability of Iceland Scotland Overflow Water Across the Reykjanes Ridge: 2-Years of Moored Observations in the Bight Fracture Zone

H. Furey<sup>1</sup> , A. Bower<sup>1</sup> , A. Ramsey<sup>1</sup>, A. Houk<sup>1</sup>, and T. Meunier<sup>1,2</sup> 

<sup>1</sup>Woods Hole Oceanographic Institution, Woods Hole, MA, USA, <sup>2</sup>Laboratoire d'Océanographie Physique et Spatiale, Université de Bretagne Occidentale, Plouzané, France

**Abstract** This study presents the first continuous observations of Iceland Scotland Overflow Water (ISOW) passing through the Bight Fracture Zone (BFZ), the northernmost deep bathymetric channel across the Reykjanes Ridge between the Iceland and Irminger Basins in the subpolar North Atlantic. Data from two 2-year moorings, measuring temperature, salinity, and current velocity from 2015 to 2017, along with a set of deep ISOW-embedded RAFOS floats, are used to investigate ISOW transport and water property variability through the BFZ, as well as advective pathways between the Iceland and Irminger Basins. The mooring-derived record-mean ISOW transport through the BFZ was  $-0.59 \pm 0.27 \times 10^6$  m<sup>3</sup>/s (westward) and varied seasonally with weaker transport in winter and stronger transport in summer. Flow direction of ISOW through the BFZ was consistently westward except in winter, when week-long flow reversals were frequently observed. The previously reported subpolar North Atlantic freshening event of the 2010s is evident in the BFZ mooring records beginning about January 2017. About one-quarter of floats deployed in ISOW at 1800-m depth upstream in the Iceland Basin show a direct advective pathway into the BFZ that appears to be primarily determined by bathymetry. Another quarter of the floats crossed over the ridge to the Irminger Sea through other gaps prior to reaching the Charlie-Gibbs Fracture Zone.

**Plain Language Summary** The deep currents in the North Atlantic Ocean transport cold, dense waters from high latitudes southward as part of the climate-relevant overturning circulation. Understanding of the pathways and transports of these currents is improving, but some knowledge gaps persist. This paper describes the first sustained measurements of the deep current transporting cold, dense water through a major gap in the shallow Mid-Atlantic Ridge, called the Bight Fracture Zone (BFZ), during 2015–2017. The resulting estimate of the mean volume transport through BFZ (about 600,000 m<sup>3</sup>/s westward) helps to quantify the total amount of this dense water mass passing from the eastern to western North Atlantic and provides a benchmark for numerical simulations of the deep ocean circulation in this region. The measurements also revealed an apparent seasonal cycle in volume transport, and unexpected flow reversals, mostly in winter. In early 2017, a significant decrease in salinity was observed, indicating the arrival in the BFZ of a known large-scale low-salinity anomaly that has been circulating around the northern North Atlantic since about 2010. Taken together, the results add several pieces to the puzzle that is the complex deep ocean circulation of the North Atlantic.

## 1. Introduction

Iceland Scotland Overflow Water (ISOW), a water mass transported by the deep limb of the Atlantic Meridional Overturning Circulation (AMOC), is the equilibrated product of dense overflow water from the Nordic Seas into the eastern subpolar North Atlantic (SPNA). It is historically defined as water with  $27.80 < \sigma_\theta < 27.88$  kg/m<sup>3</sup>, originating from the Nordic Seas and entering the Iceland Basin over the Iceland-Scotland Ridge (e.g., Dickson & Brown, 1994; Kanzow & Zenk, 2014; Beaird et al., 2013; Figure 1). Once this dense overflow water enters the Iceland Basin, it flows around the northern end of the basin, then southwestward along the eastern flank of the Reykjanes Ridge (RR), mixing and increasing in transport from 2.6 Sverdrups (1 Sverdrup, or Sv  $\equiv 1 \times 10^6$  m<sup>3</sup>/s) at the northern end of the Iceland Basin to 5.3 Sv at 59°N (Johns et al., 2021). At the latter location, ISOW is comprised of 50% overflow water that has crossed the Iceland-Scotland Ridge, and 50% Subpolar Mode Water and Labrador Sea Water in approximately equal parts (Johns et al., 2021).

ISOW continues southwestward as a deep boundary current along the eastern flank of the RR and is partially siphoned off into the Irminger Sea to the west through gaps in the ridge (e.g., Petit et al., 2022). The first major gap

Writing – original draft: H. Furey  
Writing – review & editing: H. Furey,  
A. Bower, A. Ramsey, A. Houk,  
T. Meunier

in the RR with sill depth deeper than 2,000 m is the Bight Fracture Zone (BFZ) at  $\sim 56.7^\circ\text{N}$  (Figure 1). The ISOW traveling through this gap in the ridge becomes part of the Northeast Atlantic Deep Water (NEADW; Van Aken & Becker, 1996) in the Irminger Basin, influencing the properties of waters transported by the deep limb of the AMOC in the SPNA.

Results from a 20-year HYCOM model simulation (Xu et al., 2010) showed a mean ISOW transport of  $-1.2 \pm 0.31$  Sv (westward) over the RR between about  $53^\circ\text{N}$  and  $59^\circ\text{N}$ . At the BFZ ( $57^\circ\text{N}$ ), Xu et al. found the mean transport to be  $-0.4$  Sv, and mean velocities to be  $\sim 2\text{--}5$  cm/s westward. Synoptic observational transport estimates across the BFZ range from  $-1.3 \pm 0.1$  and  $-0.3 \pm 0.1$  Sv (from Lowered Acoustic Doppler Current Profiler (LADCP) sections; Petit et al., 2022) and  $-0.8 \pm 0.8$  Sv (from geostrophic estimates; Petit et al., 2018). Using Deep-Argo profiling floats set to drift at 1,900–2,100 dbar, Petit et al. (2022) showed the westward pathway of ISOW through the BFZ. The remaining ISOW has been shown to leave the Iceland Basin westward via the Charlie-Gibbs Fracture Zone (CGFZ) near  $53^\circ\text{N}$  (Bower & Furey, 2017; Saunders, 1994; Xu et al., 2018; Zou et al., 2020) or southward into the West European Basin (e.g., Xu et al., 2010; Zou et al., 2017). There is also evidence from subsurface float trajectories that a small fraction of ISOW leaves the Iceland Basin through gaps in the RR between the BFZ and CGFZ (Lozier et al., 2022). Until now, there have been no time series observations in the BFZ (or any other fracture zone along the RR north of the CGFZ) to validate models or contextualize synoptic observational estimates.

In this study, data from two moorings equipped with conductivity, temperature, and pressure sensors paired with current meters, were used to estimate the first measured transport time series of ISOW through the BFZ, from July 2015 to July 2017. These mooring data were analyzed along with a subset of concurrent acoustically tracked RAFOS float data collected for the multi-national Overturning in the Subpolar North Atlantic Program (OSNAP; e.g., Lozier et al., 2018; Li et al., 2021; Lozier et al., 2022; Fu et al., 2023). OSNAP RAFOS floats seeded within the ISOW layer in the boundary current along the eastern flank of the RR reveal the export pathways of ISOW through the CGFZ and southward along the eastern flank of the Mid-Atlantic Ridge (Lozier et al., 2022; Zou et al., 2017, 2020). In the present work, a subset of these floats are used in conjunction with mooring data to examine the connectivity between the Iceland and Irminger Basins through the BFZ. An observationally based understanding of how the Iceland and Irminger Basins communicate with each other via the BFZ provides fundamental insight into the pathways and processes that define the subpolar AMOC system.

## 2. Data and Methods

### 2.1. Instrumentation and Data

#### 2.1.1. OSNAP Synoptic Observations and Moored Instruments

A subset of the lowered conductivity-temperature-depth (CTD) measurements and LADCP velocity data collected as part of the OSNAP program were used in this study. Specifically, data collected in the BFZ were utilized, including: one set of CTD data collected 27–28 July 2014, and two sets of LADCP data collected 27–28 July 2014 and 19 July 2016. LADCP data were collected with station spacing of 4–5 km (Figure 1). The data were processed as in Johns et al. (2021) and included the use of on-station vessel-mounted ADCP (VM-ADCP) data and bottom-track data from the LADCP to constrain the final velocity profiles. East Reykjanes Ridge (ERR) OSNAP mooring array data (Figure 1) collected continuously since 2014 were also used to validate ISOW transport calculation methods described below. Gridded mooring-derived ERR OSNAP data were used to find monthly mean velocity at the time of RAFOS float deployments.

#### 2.1.2. BFZ Moored Instruments

Two 2-year (2015–2017) moorings were placed in the central part of each of the two deep east-west channels in the BFZ from July 2015–July 2017, to measure the temperature, salinity, and velocity of ISOW as it passes through the fracture zone. The mooring positions were chosen based on a high-resolution OSNAP CTD and LADCP survey across the fracture zone in 2014 (Figure 1b) to be in the high velocity cores of each channel (Figure S1 in Supporting Information S1). Each of the two moorings deployed in the BFZ was instrumented at four depths, with one Seabird SBE37 MicroCAT CTD (hereafter, microcat) paired with a Nobska MAVS-4 current meter. These instrument pairs were placed at 1,500, 1,750, 2,000-m depth and 22 m above the bottom



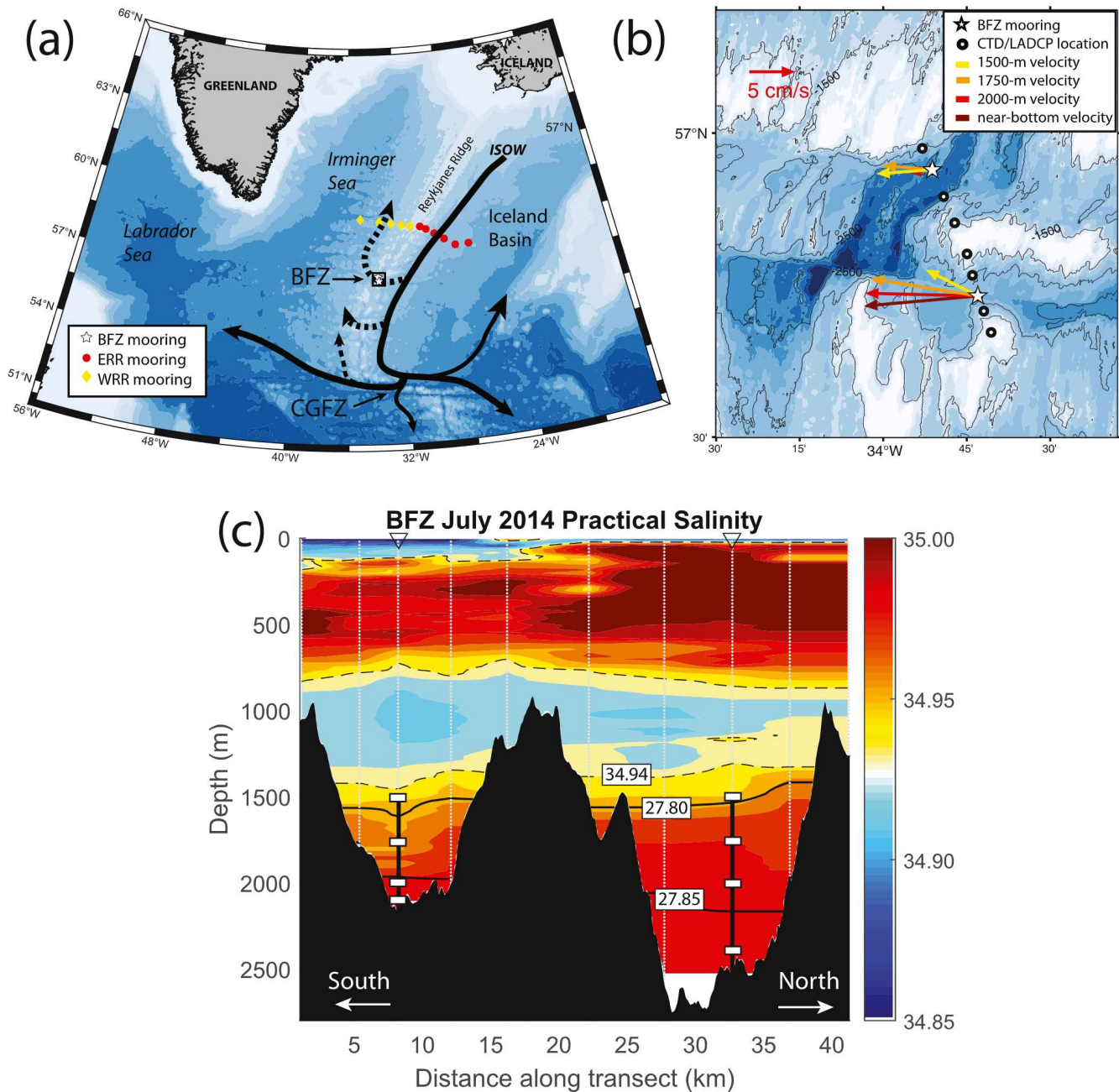


**Figure 1.** (a) Map of the SPNA with schematic Iceland Scotland overflow water (ISOW) pathways, with East Reykjanes Ridge, West Reykjanes Ridge, and Bight Fracture Zone (BFZ) mooring array locations, plotted using ETOPO2 bathymetry data. Schematic pathways for ISOW are drawn as black lines. (b) Zoom-in map of the BFZ mooring and 2014 CTD station locations, plotted over multibeam bathymetry data. Two-year mean velocity arrows are drawn at each instrument depth. (c) Schematic moorings (black vertical lines) with paired microcats and current meters (white rectangles) are drawn over practical salinity contours from OSNAP CTD data collected across the BFZ in July 2014. The  $x$ -axis distance is plotted from south to north (left to right). The 27.80 and 27.85  $\text{kg/m}^3 \sigma_\theta$  isopycnals are drawn as black lines. CTD-LADCP station locations are drawn as light gray dotted lines. The locations of the moorings are marked with triangles at the top of the figure. Bathymetry is from multibeam data collected in 2014.

of the channel at 2,440 (north channel, or “NC”) or 2,115 (south channel, or “SC”) meters depth (Figure 1c). The microcats measured time series of conductivity, temperature, and pressure at 15-min intervals, and the current meters recorded  $u$ -,  $v$ -, and  $w$ -velocity, and temperature at 2-min intervals. Continuous data were collected from 1 July 2015–20 July 2017, and averaged to hourly intervals. Instrument depths and basic statistics of measured properties are provided in Table 1. Accuracy of the pressure measurements is 0.1% of full-scale range;

**Table 1**

Mean Properties and Standard Deviations for the 2-Year, 40-hr Low-Pass Filtered Data Records From the Bight Fracture Zone Mooring Instruments

Nominal instrument depth (m)	Pressure (dbar)	Theta (°C)	Practical salinity	Potential density ( $\sigma_\theta$ , kg/m <sup>3</sup> )	Zonal velocity ( $U$ ) cm/s	Meridional velocity ( $V$ ) cm/s
BFZ-North 2,540 m depth [56.940°N 33.853°W]						
1,500	1,513 ± 0	3.55 ± 0.06	34.968 ± 0.007	27.807 ± 0.009	-5.3 ± 4.9	-3.3 ± 4.0
1,750	1,767 ± 0	3.42 ± 0.05	34.973 ± 0.005	27.824 ± 0.006	-5.1 ± 4.1	-2.1 ± 3.3
2,000	2,022 ± 0	3.32 ± 0.05	34.977 ± 0.004	27.837 ± 0.006	-2.2 ± 2.8	-1.5 ± 2.1
2,440	2,470 ± 0	3.18 ± 0.04	34.981 ± 0.003	27.853 ± 0.004	-0.6 ± 1.0	0.6 ± 1.2
BFZ-South 2164 m depth [56.733°N 33.717°W]						
1,500	1,514 ± 1	3.54 ± 0.05	34.962 ± 0.007	27.803 ± 0.008	-5.8 ± 5.6	2.7 ± 2.5
1,750	1,768 ± 1	3.36 ± 0.05	34.974 ± 0.005	27.830 ± 0.005	-12.0 ± 8.5	1.5 ± 1.6
2,000	2,023 ± 1	3.15 ± 0.06	34.983 ± 0.003	27.857 ± 0.006	-12.5 ± 9.7	-0.2 ± 1.4
2,115	2,140 ± 0	3.08 ± 0.06	34.986 ± 0.003	27.867 ± 0.006	-12.5 ± 9.3	-1.6 ± 1.5

Note. Pressure, potential temperature, practical salinity, and  $\sigma_\theta$  data are from Seabird SBE37 MicroCATs. Velocity data are from Nobska MAVS-4 current meters.

temperature is  $\pm 0.002^\circ\text{C}$ ; the derived practical salinity is  $\pm 0.003$ ; and velocity is  $\pm 0.3$  cm/s. A full description of these data, including quality control and calibration, may be found in Furey et al. (2024a).

For the transport calculations, velocities were rotated into along- and across-channel components, by  $27.8^\circ$  and  $2.1^\circ$  in a Cartesian reference frame, in the NC and SC, respectively.

### 2.1.3. Absolute Dynamic Topography

Daily absolute dynamic topography (ADT) and derived variables were downloaded from Copernicus Marine Environmental Monitoring Service (CMEMS) (Taburet et al., 2019) for the mooring and RAFOS float observational period, 2014–2019.

### 2.1.4. Argo Floats

Delayed-mode Argo float data were accessed from the data storage site US-GODAE (Global Ocean Data Assimilation Experiment), from 01 January 2015 through 31 December 2017 and within the bounds  $55.15^\circ\text{N}$ – $58.75^\circ\text{N}$   $29^\circ\text{W}$ – $39^\circ\text{W}$ . Temperature and salinity profile data from 35 Argo floats were used in the analysis below.

### 2.1.5. RAFOS Floats

As part of the OSNAP program, a total of 135 acoustically tracked isobaric RAFOS floats (Rossby et al., 1986) were deployed between 2014 and 2017 at overflow water depths (1,800–2,800 m) at various sites throughout the SPNA. The floats were ballasted and positioned to tag ISOW and DSOW transported by the SPNA deep boundary currents, including across the eastern flank of RR at about  $59^\circ\text{N}$ . A technical description of the OSNAP RAFOS float program can be found in Ramsey et al. (2020), and data can be found in Furey and Ramsey (2019). The RAFOS floats recorded daily pressure, temperature, and acoustic times-of-arrival data from an array of moored sound sources, yielding eddy-resolving trajectories with nominal 2-year duration. All RAFOS floats used in this study were confirmed at launch to be embedded in the ISOW layer (density  $> 27.8$  kg/m<sup>3</sup> at float ballast pressure) using concurrent CTD profiles.

To determine if the RAFOS floats were continuously embedded in the ISOW layer as they drifted throughout the BFZ region, we did a regional census of the depth of the  $27.8$  kg/m<sup>3</sup>  $\sigma_\theta$  isopycnal from Argo profile data during the study period. The  $27.8$  kg/m<sup>3</sup>  $\sigma_\theta$  depth distribution east of the RR is between 1,200 m and 1,600 m, while west of the RR, the distribution ranges from 1,200 m to 2,000 m (Figure S2 in Supporting Information S1). The distribution is noisier on the west side of the RR compared to the east, for example, west of the RR,  $27.8$  kg/m<sup>3</sup>  $\sigma_\theta$  depth was observed at 1,200 m adjacent to another profile where it was observed at 1,700–1,800 m ( $57.5^\circ\text{N}$   $34.5^\circ\text{W}$ ). At the West Reykjanes Ridge (WRR) mooring array, the mean depth of the  $27.8$  kg/m<sup>3</sup>  $\sigma_\theta$  surface is at approximately 1,700 dbar, above the depth of the shallowest RAFOS floats (de Jong et al., 2020; Fried and de Jong, 2022). We



conclude from these results that the RAFOS floats were generally embedded in ISOW as they drifted through the BFZ and into the Irminger Sea.

### 2.1.6. Multibeam Bathymetry

Multibeam bathymetry data from the BFZ region can be found at NOAA's National Centers for Environmental Information (NCEI), under Survey ID MGL1309 (Hey et al., 2016).

## 2.2. Defining Upper Boundary of ISOW Layer in BFZ

During the 2-year BFZ mooring deployment, the  $\sigma_\theta = 27.80 \text{ kg/m}^3$  top boundary of the ISOW layer (unexpectedly) often rose above the depth of the top mooring instruments (1,500 m). This occurred 78% and 67% of the time in the NC and SC, respectively. These events were sometimes short, a few days or weeks, but during the winter, such events were months long. In general, between November and May, the  $27.80 \text{ kg/m}^3$   $\sigma_\theta$  isopycnal was continuously above 1,500 m for both channels. This issue needed to be addressed in order to estimate transport of ISOW through the fracture zone from the mooring observations. When the isopycnal was shallower than the 1,500-m mooring instrument, we estimated the depth of this isopycnal as follows. First, we identified an isopycnal that remained deeper than the top instrument in both channels for the entire 2-year period,  $\sigma_\theta = 27.825 \text{ kg/m}^3$ . Next, we identified times when both isopycnals were deeper than the top mooring instruments, and calculated the difference in pressure between  $\sigma_\theta = 27.800$  and  $27.825 \text{ kg/m}^3$  for each mooring separately. This resulted in a mean layer thickness, or “ $\Delta\text{PR}$ ”, of  $342 \pm$  one standard deviation of 83 dbars in the NC, and  $189 \pm 24$  dbars in the SC (Figure S3 in Supporting Information S1). The pressure of the  $27.80 \text{ kg/m}^3$   $\sigma_\theta$  surface was then estimated for each time step using its interpolated pressure value when deeper than 1,500 dbar, or extrapolating its pressure value defined as  $\text{PR}_{27.825} - \Delta\text{PR}$  when it was above 1,500 dbar, where both  $\text{PR}_{27.825}$  and  $\Delta\text{PR}$  are specific to each mooring. We will refer to this estimated pressure record as “uncapped”. The mean of the uncapped pressure records over the measurement period was 1,456 dbar for the NC and 1,501 dbar for the SC. We will refer to the “capped” method as using the pressure of the 1,500-m microcat as the top of the ISOW layer when the  $\sigma_\theta = 27.80 \text{ kg/m}^3$  isopycnal is shallower than the top instrument.

This methodology assumes that the density gradient between 27.800 and 27.825 at each mooring site is constant in time. We checked this assumption in two ways: first by estimating  $\Delta\text{PR}$  from Argo data collected during the study period to examine the BFZ mooring  $\Delta\text{PR}$  in a geographic context, and, second, by estimating  $\Delta\text{PR}$  from OSNAP ERR moorings to look at the variability of  $\Delta\text{PR}$  over time. The mean and standard deviation of  $\Delta\text{PR}$  at various mooring sites are summarized in Table S1 in Supporting Information S1.

The Argo-derived  $\Delta\text{PR}$  shows that  $\Delta\text{PR}$  varied across the region (Figure S4 in Supporting Information S1), and that the values calculated at the BFZ and ERR moorings fit into this regional pattern. The OSNAP ERR mooring data, which had continuous 2-year records with the top instrument (1,200-m depth) always above the  $27.8 \text{ kg/m}^3$   $\sigma_\theta$  isopycnal, appear to have no seasonal signal in  $\Delta\text{PR}$  (Figure S5 in Supporting Information S1, mooring D2 shown as an example). These results support our method for estimating  $\Delta\text{PR}$ . The standard deviation of the BFZ mooring  $\Delta\text{PR}$  is used to put error bounds on the transport estimate (Tables S1 and S2 in Supporting Information S1), and is discussed below.

### 2.3. Equivalent Width Transport Method

To estimate ISOW transport from the mooring data, we first consider the bathymetry of the BFZ: it is divided into two deep channels, separated by a 924-m deep median ridge, with maximum depth at the mooring longitude of 2,168 m in the SC and 2,756 m in the NC. Each channel is about 15–20 km wide (Figures 1b and 1c, Figure S1 in Supporting Information S1). At the meridional location ( $\sim 33.75^\circ\text{W}$ ) across the BFZ, the ISOW layer ( $\sim 1,500$  m depth to the seafloor) has been observed to be well beneath the top of the median ridge depth. Therefore, the transport time series for the NC and SC were calculated separately. East of the mooring longitude, the two channels remain separated by the median ridge. About 15 km west of the moorings, the two channels join. Note that the NC mooring (Figure 1c) is not located in the deepest part of the channel, it is in the region of strongest velocity as measured from LADCP in July 2014 (Figure S1 in Supporting Information S1). Also note that although there is no data from 2,440 to 2,756 m depth, the 2-year 2,440 m velocities are weak,  $<1$  cm/s in the mean. We therefore assume that there is no strong flow below this instrument within this geographically isolated deep portion of the NC.

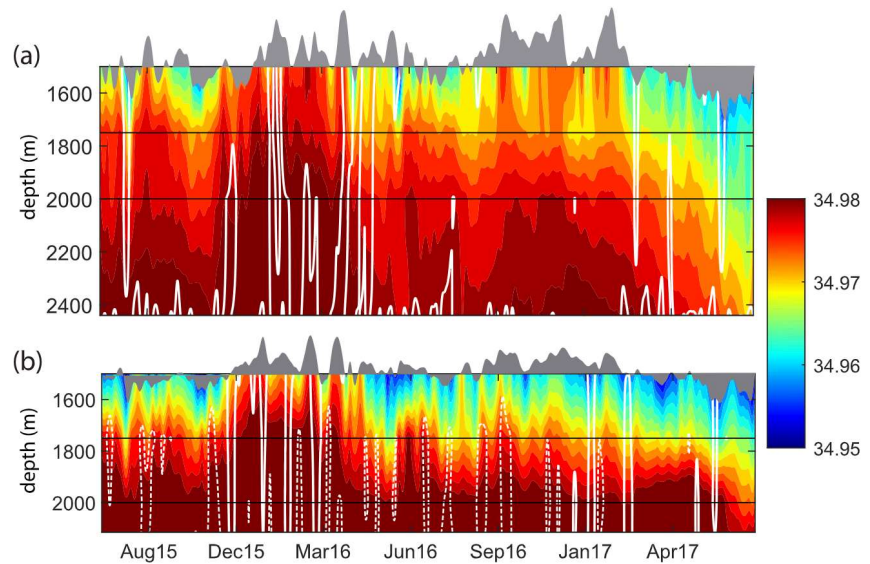


**Figure 2.** Profiles of practical salinity in the (a) NC and (b) SC plotted versus time. Along-channel speed is contoured in white: zero velocity is rendered as a solid line and  $-20$  cm/s as a dashed line. Instrument locations are marked with thin black horizontal lines. The uncapped depth of the Iceland Scotland overflow water layer, that is, the  $27.80 \text{ kg/m}^3 \sigma_\theta$  isopycnal, is shown as a gray patch.

ISOW transport was estimated from the BFZ mooring data using the “equivalent width” method developed by Johns et al. (2003). Equivalent width is derived from an average of synoptic transport estimates based on LADCP section data. The equivalent width is then mapped onto a mooring velocity time series, yielding an estimate of transport over time. The assumption being that the cross-channel structure of velocity is generally time-invariant, that is, the velocity core is generally in the same spatial location over the time period of the analysis.

Specifically, equivalent width,  $W_e(z)$  is related to transport by

$$V(z) = W_e(z) \times v_0(z)$$

where  $V(z)$  is the transport per unit depth,  $v_0(z)$  is the mid-channel (mooring site) velocity per unit depth,  $W_e(z)$  is a parameter with units of length that accounts for the physical width of the channel at each depth as well as the actual velocity structure across the channel. The transport time series is then calculated as follows:

$$T(z) = W_e(z) \times V(z) \times H$$

where, at a depth  $z$ ,  $W_e$  is the equivalent width,  $V$  is the velocity, and  $H$  is the depth bin value.

### 3. Results

#### 3.1. Velocity and Water Properties in the BFZ

The 2-year mean zonal speed at all instruments is westward at both mooring sites (Figure 1b and Table 1). The along-channel (rotated) mean speed for the NC was strongest at the 1,500-m (top) instrument ( $-6.2$  cm/s) and similar in magnitude to the 1,500-m instrument in the SC ( $-6.4$  cm/s). NC mean along-channel speed decreased with depth,  $-5.5$  cm/s (1,750-m),  $-2.6$  cm/s (2,000-m), and  $-0.8$  cm/s (2,440-m). In contrast, SC mean along-channel speeds were larger and near uniform below the 1,500-m instrument, at  $-12.1$  cm/s (1,750 m),  $-12.5$  cm/s (2,000 m), and  $-12.6$  cm/s (2,115 m). Along-channel speed shows that velocity variability at all depths is, in general, uni-directional (Figure 2, white contours; Figures 3d and 3h). Zonal flow reversals, more prevalent in winter months, were measured at all four instruments simultaneously, and were typically  $\sim 1$  week in duration. The maximum daily mean velocities were observed in the SC from 1,750 m to the seafloor, with week-long pulses of strong westward velocity ( $< -20$  cm/s) throughout the mooring record (Figures 3d and 3h).



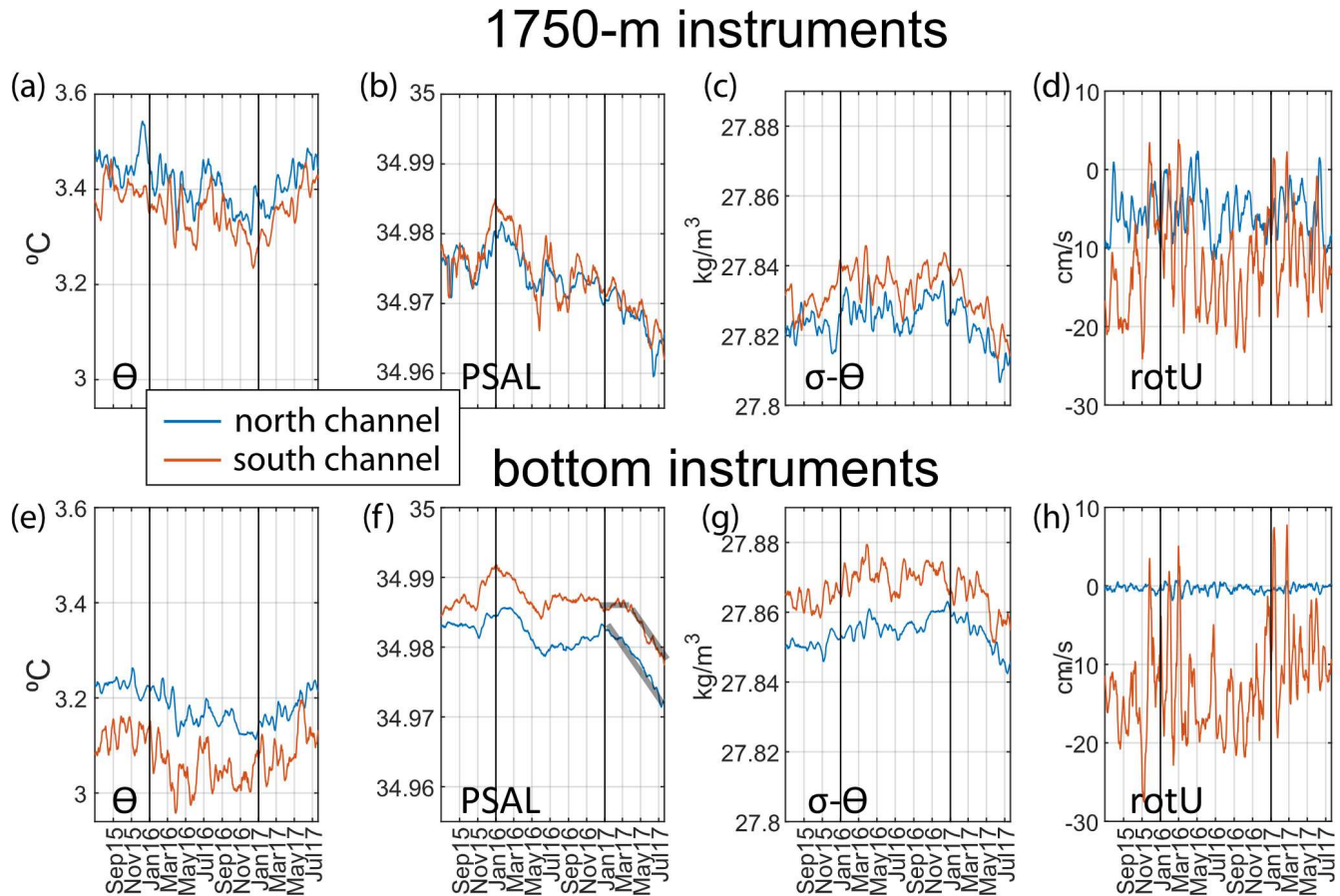


**Figure 3.** Two-year records of daily mean (a, e) potential temperature (b, f) practical salinity (c, g) potential density, and (d, h) along-channel speed for the NC (blue) and SC (orange) at instrument depths of 1,750 m (top row) and at the bottom instrument (bottom row). The bottom instrument was at 2,440 m in the NC, and 2,115 m in the SC.

Temperature, salinity, and density are notably different between the two channels over the 2-year study period. Mean potential density at all instruments is greater than  $27.8 \text{ kg}/\text{m}^3$ . Although the mean potential density at 1,500 m is essentially the same in both channels, all deeper instruments in the NC persistently recorded less dense water (warmer and fresher) than in the SC, by  $0.01\text{--}0.02 \text{ kg}/\text{m}^3$  in the mean (Table 1; Figure 3).

Salinity hovmöller plots for each channel illustrate dynamic changes of salinity over the 2-year period (Figure 2). There is a salinification of the water column from December 2015–April 2016, where increased salinity of about 0.01 is measured at all depths and in both channels. This salinification event coincides with an enhanced period of zonal flow reversals. Also notable is the freshening of ISOW in the last months of the 2-year record, which is measured by all instruments, and in both channels. This freshening event, up to 0.02, becomes pronounced in ~January 2017 in the NC, and ~April 2017 in the SC.

The freshening event in winter-spring 2017 is uncompensated by temperature, so density decreased in both channels (Figures 3c and 3g), with the lowest densities in the 2-year records measured during this time, particularly for the NC. Temperature (increasing) and salinity (decreasing) both act to reduce the density during the freshening event period January–July 2017. Although temperature appears to effect both channels at the same rate (especially at 1,750 m, Figure 3a), the salinity affects each channel at different rates or at different times (see gray lines in Figure 3f), when the NC becomes fresher several months prior to the SC. Overall, these effects lead to a weaker SC freshening when compared to the NC over the same period.

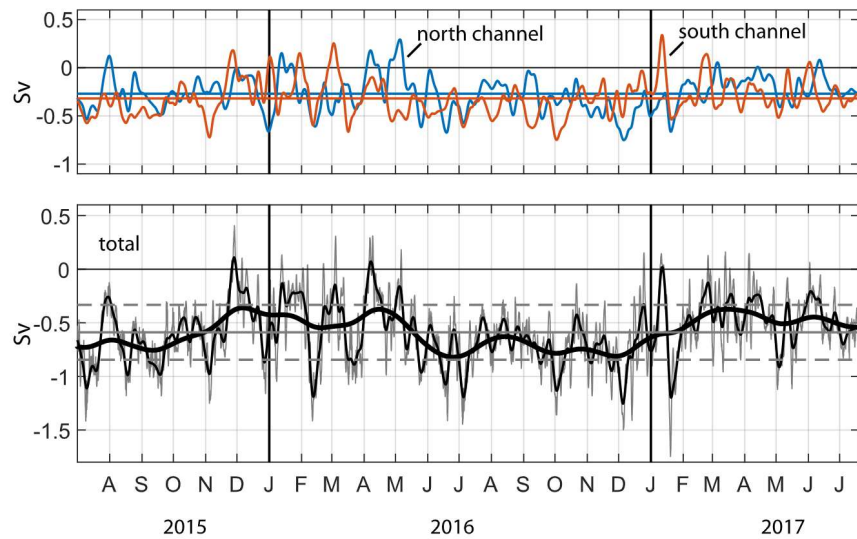


**Figure 4.** Two-year Iceland Scotland overflow water transport time series from the Bight Fracture Zone (BFZ) moored instrument data. Top panel: 10-day low-pass filtered transport time series for the SC (orange) and NC (blue) individually. Record mean values are drawn as straight orange and blue lines. Bottom panel: Daily mean total transport through the BFZ with low-pass filter cut-off periods of 40 hr (thin gray line), 10 days (thin black line), and 90 days (thick black line). Dashed and solid straight gray lines mark record mean and standard deviation.

### 3.2. ISOW Transport Through BFZ

Mean 2-year transport through the BFZ was  $-0.59$  with a standard deviation of  $\pm 0.27$  Sv, with almost equal transport distribution (within uncertainties) between the two channels (Figure 4 and Table 2;  $-0.27 \pm 0.22$  Sv for the NC and  $-0.32 \pm 0.23$  Sv for the SC). Across both channels, the maximum transport was  $+0.41$  Sv and minimum was  $-1.75$  Sv. ISOW transport through the BFZ was westward 97% of the time.

Transport sensitivity to the use of capped versus uncapped pressure, and the variability of both  $\Delta PR$  and  $W_e$ , on transport estimates yield mean BFZ transport ranging from  $-0.44$  Sv to  $-0.74$  Sv (Table S2 in Supporting Information S1). The mean westward transport was  $-0.07$  Sv more westward for the uncapped method compared to the capped. Differences were greater for the NC transport compared to the SC, where capped transports were 78% and 97% of the uncapped values, respectively. This difference is the result of more frequent and shallower extrapolated pressure values for the  $27.8 \text{ kg/m}^3$  isopycnal in the NC. Allowing the uncapped pressure to vary by  $\pm$  one standard deviation results in mean transport variation of  $\sim 0.05$  Sv, from  $-0.54$  to  $-0.63$  Sv, respectively. The transport resulting from using the minimum and maximum  $W_e$  profiles, for example, using different LADCP section data, results in transport ranging from  $-0.44$  to  $-0.74$  Sv, which is about a  $\pm 25\%$  difference in the mean value.

We compared the ISOW transport estimated from mooring data to contemporaneous synoptic estimates reported by Petit et al. (2018), who calculated from shipboard ADCP referenced geostrophic velocities derived from CTD profiles. Their estimate of  $-0.8 \pm 0.8$  Sv resulted from data collected over a 3.6-d window (29 June 2015

**Table 2**  
Mean and Standard Deviation of Iceland Scotland Overflow Water Transport for the 40-hr Low-Pass Filtered 2-Year Records

ISOW transport estimates	Mean and STD (Sv)	Maximum (Sv)	Minimum (Sv)	Percent time westward
Method		Pressure uncapped		
North channel	$-0.27 \pm 0.22$	0.56	-1.02	90%
South channel	$-0.32 \pm 0.23$	0.54	-1.00	89%
Overall Bight	$-0.59 \pm 0.27$	0.41	-1.75	97%

Note. Maximum and minimum transport as well as % time westward are also presented.



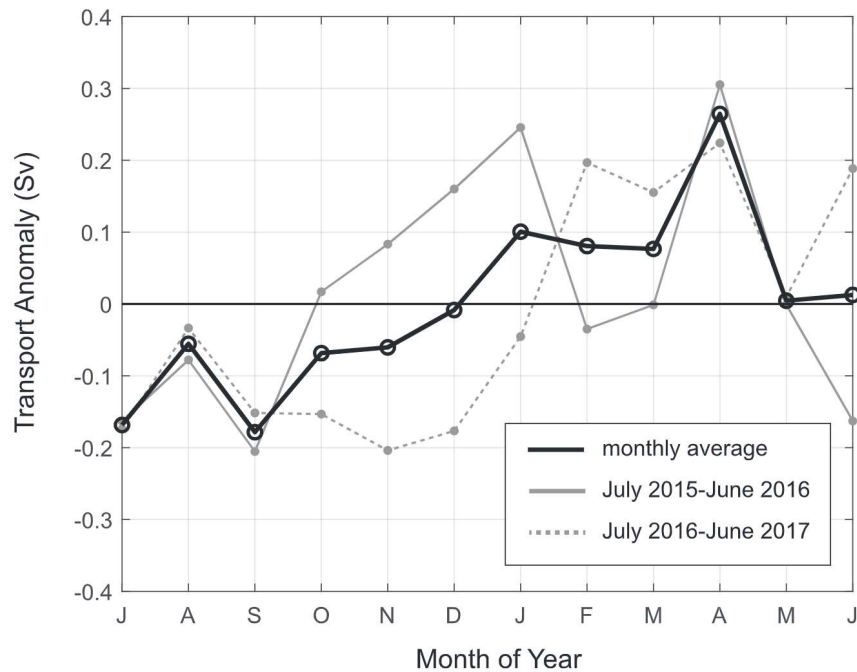


**Figure 5.** Monthly mean Bight Fracture Zone transport anomaly for year 1 (July 2015–June 2016), year 2 (July 2016–June 2017), and the 2-year average.

17:51UTC to 07 July 15:43UTC). The mean mooring-derived ISOW transport for this time period was  $-0.77 \pm 0.13$  Sv. The two estimates agree well within uncertainties. Petit et al. (2022) also estimated transport across the SC in August 2017, a few weeks after the moorings were recovered. Their estimate of  $-0.5 \pm 0.2$  Sv is close to the mooring-derived estimate of  $-0.45$  Sv on the last day of the mooring record. This may be fortuitous considering the higher frequency oscillations often observed in the 2-year record.

The general character of transport for the 2-year mooring period (Figure 4) is of stronger westward transport ( $\sim -0.8$  Sv) in July–November, and weaker westward transport ( $\sim -0.3$  Sv) in winter through spring. Superimposed on these months-long transport changes are large amplitude oscillations of a few weeks duration: the most extreme example occurred in January 2017, when transport was weakly eastward at 0.1 Sv in mid-January, and strongly westward at  $-1.7$  Sv about one week later. The transport time series generally shows larger amplitude transport oscillations in the  $\sim$ December–April than in  $\sim$ July–November, with winter transport variability of about 1 Sv over 1-month time periods, while summer variability is generally about half that amount. Spectral analysis on the three time series (NC, SC, and total) did not yield significant spectral peaks of variability over this 2-year observing period (not shown).

Transport variability in the two channels is sometimes in phase (e.g., July 2015 and July 2016, when both channels have a westward maximum) and sometimes out of phase (e.g., March and May 2016, when one channel has an eastward maximum, and the other channel has a westward maximum). Overall, the NC and SC daily mean transport time series are statistically uncorrelated at all lags ( $r < 0.3$ ). Transport is correlated with along-channel vertically integrated velocity in each channel at 0-day lag, strongly in the SC ( $r = 0.87$ ) and moderately in the NC ( $r = 0.46$ ). Both channel transport records are uncorrelated at 0-day lag with ISOW layer thickness (both with  $r < 0.3$ ), defined as the daily averaged height between the 27.8 isopycnal (uncapped) and the seafloor. There was no correlation between the time series of sea-surface height difference across the fracture zone (from  $57.25^\circ\text{N}$   $33.50^\circ\text{W}$  to  $56.25^\circ\text{N}$   $34.50^\circ\text{W}$ ) and ISOW transport.

### 3.3. Annual Signal

The apparent annual cycle in ISOW transport through the BFZ for this 2-year period is explored by calculating monthly mean averages of transport and finding the 2-year monthly mean transport anomaly (Figure 5). These results suggest that the ISOW transport through the BFZ is stronger from July–November and weaker January–

April, with transitions in December and May–June. There is evidence of a seasonal cycle in a 34-year record of model-derived ISOW transport along the northern slope of the Iceland Basin and across the RR, with stronger (weaker) transports occurring in summer (winter) (Xu et al., 2018; their Figure 15). In that study, a winter/summer weaker/stronger ISOW transport signal is found in integrated transport sections across the Iceland Basin from south of the Iceland-Scotland Ridge to a 58°N section, and also along the crest of the RR.

### 3.4. ISOW Pathways to and From the BFZ

We next investigate the ISOW pathways upstream and downstream of the BFZ as revealed by OSNAP RAFOS floats released along the ERR OSNAP Section 100–200 m above the bottom between the 1,850-m and 2,700-m isobaths in 2014, 2015 and 2016 (Figures 1 and 6). Drifting at nominal pressures from 1,800 to 2,500 dbar, the floats generally moved southwestward after launch, parallel to the isobaths over the eastern flank of the RR to the CGFZ, with some floats crossing the ridge upstream at either the BFZ or “no-name gap” (NNG) (Lozier et al., 2022). Other floats drifted eastward into the central Iceland Basin. Only 1,800-dbar floats crossed the ridge upstream of the CGFZ, so we restrict the analysis here to those floats. Floats in this subset were deployed at the three sites closest to the RR crest, and all were clearly embedded in the ISOW upper plume at launch according to concurrent CTD profiles (Johns et al., 2021). Sill depths are estimated from multibeam data to be 1,750 m in the northern channel and 2,150 m in the southern channel.

About 50% of the 1,800-dbar floats released at ERR (9 out of 19) crossed the RR north of the CGFZ: BFZ (4 floats: 1 in 2014, 2 in 2015, 1 in 2016); NNG (2 floats: 1 in 2014, 1 in 2015); between the BFZ and NNG (3 floats: 2 in 2015, 1 in 2016). Sound source signals used for float tracking were often blocked by the convoluted and mountainous bathymetry of the RR, and in many cases, made it impossible to track the floats continuously over the RR.

Floats deployed from the ERR site, and which crossed the RR north of the CGFZ, were twice as likely to end up north (6 floats) as they were to end up south (3 floats) of their ridge-crossing latitude, indicating a tendency to drift northward after crossing the RR. However, these floats exhibited much more eddying motion after crossing the ridge compared to more isobath-following trajectories before crossing the ridge. After 2 years, the float trajectories fill the central Irminger Sea from the RR to the eastern flank of the interior cyclonic recirculation gyre (e.g., Lavender et al., 2005), and south to the northern edge of the NAC (Figure 6; roughly from 49°N to 61°N, and 35°W to 42°W).

Float deployment locations were superimposed on velocity from mooring data for each year of deployment (Figure 7). Using similar color coding, Figure 6 shows that the locations where the floats crossed the RR are not correlated with deployment location. For example, in June 2015, floats that traveled through the BFZ to the Irminger Basin (magenta trajectories in Figure 6, magenta triangles in Figure 7) were launched farther east than floats that crossed the ridge south of the BFZ. In July 2016, the most inshore float did not cross the RR at all, while one float released farther east crossed through the BFZ. Similarly, there is no apparent correlation between speed of float, distance from ridge crest, or height above seafloor at the ERR deployment site and the float transit through the BFZ (not shown).

What does appear to influence whether the floats cross the RR through the BFZ is the location of the float just north of the fracture zone. Floats appear to be funneled into a region bounded by the RR to the northwest and a bathymetric west-east spur shallower than 2,000 m that extends from the center of the BFZ at 34°W eastward to about 31.5°W (Figure 5b, at approximately 57°N 33°W). This bathymetric feature, outlined by the 2,000 m isobath, appears to direct the water southwestward toward the BFZ. Not all the floats that are funneled in this manner travel through the BFZ, but all floats that travel through the BFZ are funneled in this way, and are the westernmost floats at this latitude, approximately 250 km downstream of the ERR deployment site. Floats with well-resolved trajectories all traveled through the BFZ via the SC; the floats were likely too deep to get over the shallower sill of the NC.

The floats drifting southward from the ERR array to the BFZ, along the flank of the RR, did so at maximum speeds of over 15 cm/s (Ramsey et al., 2020), and with mean speeds about 10 cm/s (Zou et al., 2023). Floats took an average of 66 days  $\pm$  36 days to reach the BFZ. Mean float speeds from the BFZ to the CGFZ, along the eastern flank of the RR, were about half the speed observed northeast of the BFZ, at  $\sim$ 5 cm/s. Once across the ridge the float speeds are much weaker through all pathways (BFZ, NNG, etc.), just a few cm/s in the mean, and with a



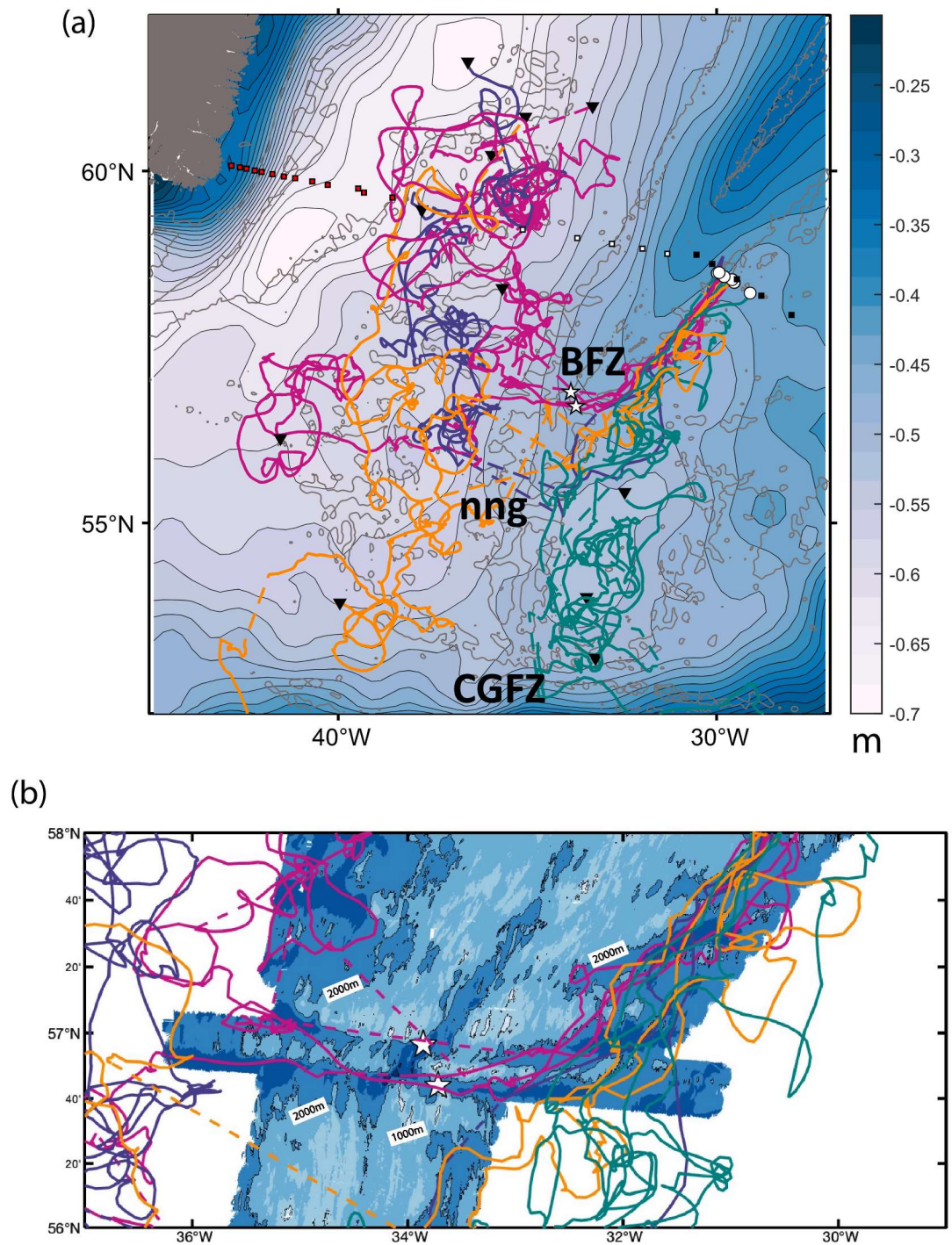


**Figure 6.** (a) Nominal 1,800-dbar float trajectories plotted over contoured 2015–2017 mean absolute dynamic topography as an indicator of the mean surface geostrophic circulation, is included to give context to the spread of the float trajectories. Floats are color-coded by behavior at the RR: magenta, crossed through the Bight Fracture Zone (BFZ); purple, crossed through the no-name gap (NNG); orange, crossed between the BFZ and NNG, or spent time at both sites; teal, did not cross the Reykjanes Ridge. White circles, float launch positions; black triangles, float surface positions; black squares, East Reykjanes Ridge mooring positions; white squares, West Reykjanes Ridge mooring positions; red squares, OSNAP East Greenland mooring sites; white stars, BFZ mooring positions. Dashed lines connect float trajectory segments where tracking was lost. ETOPO2 bathymetric contours are drawn at 1,000, 2,000, and 3,000 m. (b) As in (a), but float trajectories plotted over multibeam bathymetry and zoomed in to illustrate floats entering and exiting the BFZ. One orange-category float segment (after it traveled past the BFZ) was truncated for visual clarity. Bathymetry shaded at 500-m intervals, with the 1,000-m and 2,000-m isobaths drawn in black.



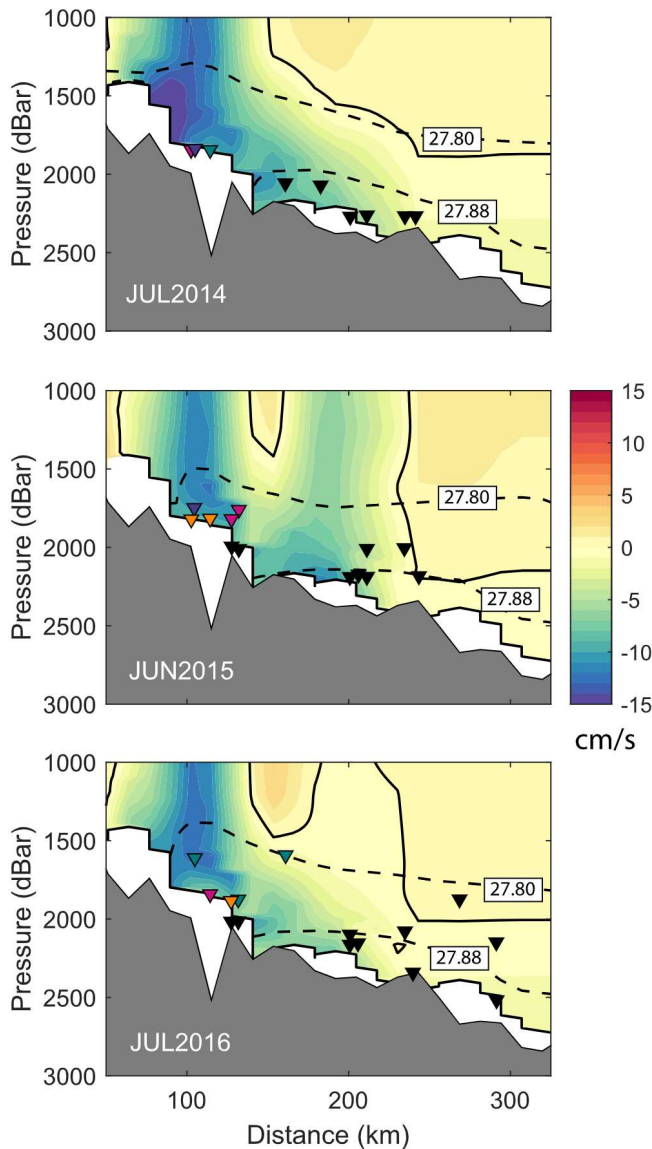


**Figure 7.** RAFOS float deployments at the East Reykjanes Ridge (ERR) site by deployment year. Floats are plotted by mean pressure of the first 100 days of deployment, and color coded by behavior at ridge, as in Figure 6: magenta, crosses through Bight Fracture Zone (BFZ); purple, crosses at no-name gap (NNG); orange, crosses ridge between BFZ and NNG (at 55°N) or as a combination of both; teal, does not cross ridge north of Charlie-Gibbs fracture zone (CGFZ) or remains in Iceland basin. None of the deeper OSNAP floats (>1,800 dbar; black triangles) crossed the ridge north of the CGFZ. They are included in the figure to illustrate their cross-slope position and pressure relative to the 1,800-dbar floats. Gridded mooring-derived month-long mean velocities normal to array of each deployment are contoured in background, showing location of the ERR current and Iceland Scotland overflow water plume. The solid black line denotes the zero-velocity contour. The dashed lines show the 27.80 and 27.88 kg/m<sup>3</sup>  $\sigma_\theta$  isopycnals. Bathymetry is from the ETOPO2 database.

more disorganized pattern. The lack of evidence for a continuous boundary current from the exit of the BFZ northeastward along the western flank of the RR is consistent with the very weak mean flows observed in WRR mooring data (de Jong et al., 2020; Fried and de Jong, 2022) at the comparable float pressures. It is also self-consistent with the findings of Lozier et al. (2022) who used all the OSNAP RAFOS float data, including the subset of floats explored in this study. The trajectories of the floats that remain in the Iceland Basin meander along the eastern RR to the CGFZ, with some floats recirculating within the southwestern Iceland Basin.

Two 1800-dbar RAFOS floats had well-resolved tracking through the BFZ (Figure 8; floats 1,358 and 1,396). Both trajectories show a relatively straight-line path through the BFZ from east to west. Both entered the BFZ by slipping into the bathymetric funnel at the entrance of the SC, as previously described, passed by the mooring in the SC, and exited the BFZ, one to the north and one to the south of a short ridge that splits the outflow at that point. Once in the Irminger Basin, the float that exited to the south continued meandering southward. The float that exited to the north followed a small meander, completed one anticyclonic rotation and then meandered farther to the north.

Previous work has shown that ADT patterns are correlated with deep flow in some locations around the SPNA, specifically in regions with strong ADT gradients like along the NAC, including in the CGFZ (Bower et al., 2022; Bower & Furey, 2017; Xu et al., 2018; Zhou et al., 2018). We looked for visual correspondence between synoptic ADT and float trajectories around the BFZ and found none.

#### 4. Discussion and Summary

During 2015–2017, two 2-year moorings were positioned in the north and south channels of the BFZ, instrumented with current meters and microcats from 1,500 m to near the seafloor, continuously measuring the temperature, salinity, and velocity of ISOW through the northern-most deep fracture zone connecting the Iceland and Irminger Basins at ISOW levels. The 2-year mean ISOW transport ( $\sigma_\theta > 27.8 \text{ kg/m}^3$ ) across both BFZ channels was  $-0.59 \pm 0.27 \text{ Sv}$ , with nearly equal transport flowing through both channels in the mean. The transport over the 2-year period exhibited several week-long intervals of complete reversal—in all but one instance, in the winter months. No eastward ISOW flow or transport has been previously reported, most likely because all prior transport estimates were based on synoptic, ship-based observations during summer months.

During this 2-year period, the westward transport is generally stronger in summer and weaker in winter. In addition to the Xu et al. (2018) modeled ISOW transport annual cycle previously mentioned, Hansen and Østerhus (2007) reported annual cycles in velocity, interface height, kinematic overflow (defined as volume flux below the interface), and temperature in the ISOW overflow through the Faroe Bank Channel, with maximum overflow transport in late summer. It may be fruitful to investigate the annual signal found in the BFZ time series, along with model and upstream observations, to explore the phasing of the signal at locations from the Faroe Bank Channel downstream to the CGFZ.

We looked at the sea-surface height difference across the fracture zone over time and found no significant correlation with ISOW transport. Johns et al. (2021) also did not find a robust link between ISOW transport record at the ERR array and the SSH slope across the array, yielding inconclusive results about any potential surface expression of ISOW transport variability at that location.



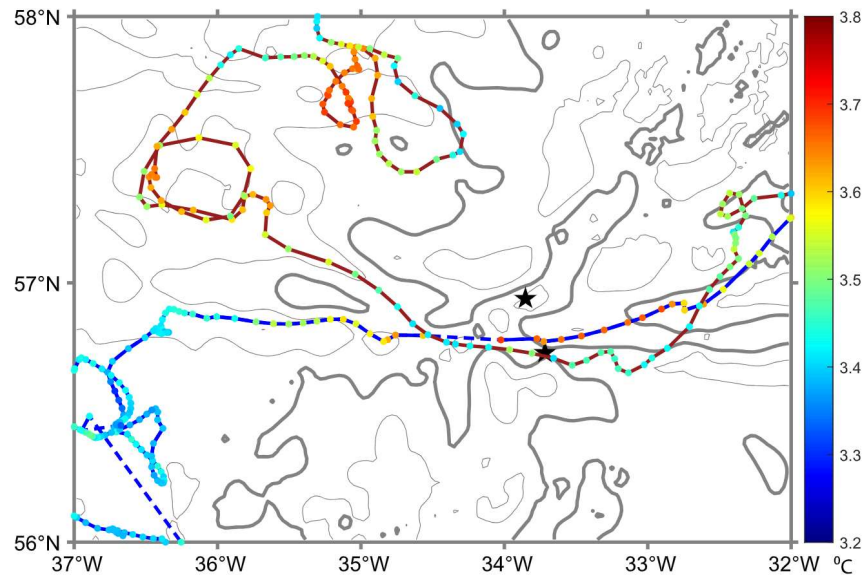


**Figure 8.** Two 1,800-m RAFOS floats returned well-resolved trajectories through the Bight Fracture Zone (BFZ). Daily float positions are color coded by temperature. The blue float passed through the BFZ in August–October 2015, and the red float passed through August–October 2016. Dashed line segments indicate when tracking was lost. The BFZ mooring locations are drawn as black stars. The bathymetry is contoured every 500-m and the 2,000-m isobath has been highlighted with a thick gray line.

The water properties of ISOW in each channel were consistently different over the 2-year period. With its shallower sill depth, the NC appears to siphon off lower-density ISOW from the main plume farther northeast in the Iceland Basin. The depth of the mean velocity maximum in each channel was different, with maximum mean velocity at the 1,500-m and 1,750-m instruments in the NC, compared with maximum mean velocity at the 1,750-m, 2,000-m, and 2,115-m instruments in the SC. This is likely due to the difference in upstream sill depths and may be the reason the NC persistently transports less dense water—the jet of high velocity is shallower in the water column at this location. As seen in Koman et al. (2020), less dense ISOW (shallower in the water column) crosses the RR farther north than the denser ISOW (see Figures 9 and 10a in Koman et al., 2020), as these first continuous time series observations in the BFZ confirm.

A notable ISOW freshening was observed in the final few months of the BFZ mooring salinity records, from January through July 2017. This is attributed to the low-salinity anomaly documented in the SPNA by Holliday et al. (2020), first apparent in 2012 in the upper 200 m off Labrador. Holliday et al. (2020), using the EN4 gridded climatology, showed the progression of this low-salinity signal at depths 0–1,000 m, from west to east across the subpolar North Atlantic into the Iceland Basin. The anomaly, stronger in the Iceland Basin than the Great Salinity Anomaly of the mid-1960s, spread through the Basin by summer 2016, where the salinity from 0 to 200 m across the basin was 0.45 salinity units less in 2016 than in 2014 (from 35.50 to 35.05). Devana et al. (2021) showed that this same signal was entrained in the overflow waters south of the Faroe Bank Channel starting in September 2015, and then observed at ERR moorings in January 2017, around the same time it first appeared in the BFZ NC.

The January–July 2017 BFZ freshening signal is evident in all microcat instruments, first in the NC and then about 3 months later (starting in April 2017) in the SC. This may reflect a time delay for the low-salinity anomaly to mix deeper into the water column: the fresh signal first reaching the shallower flow of ISOW in the NC, and later reaching the deeper water column in the SC. Alternatively, the signal may just reach the NC before it reaches the southern channel due to the longer path to reach the entrance to the SC.

Prior to the arrival of the low-salinity anomaly in 2017, a distinct high-salinity anomaly was observed in the ISOW layer in the BFZ from November 2015 to April 2016. The water column in both channels gets gradually saltier, until the salinity measures  $\sim 0.15$  salinity units higher than the mean of each channel, with peak salinity difference in January 2016. In contrast to the freshening event, the salinification occurs simultaneously in both channels, and with equal magnitude. This could be due to salinity changes in the source water at or upstream of the

Iceland-Scotland Ridge, however, this is hard to reconcile with observed lag in the arrival of the later freshening signal in the SC compared to the NC. Such variability in source water properties from the Faroe Bank Channel have been reported previously (e.g., Hansen & Østerhus 2007; Devana et al., 2021) and references therein, or the ISOW flow reversals during this period may be a factor. The water in the Irminger Sea (NEADW) is less salty than water to the east of the RR (Petit et al., 2022), so this is likely not the source of the observed salinification. An on-going analysis by OSNAP investigators of ISOW water mass composition that includes the ERR and BFZ records may shed light on these questions.

RAFOS floats released in the ISOW layer over the eastern flank of the RR upstream of BFZ were used to investigate the connectivity between the Iceland and Irminger Basins through BFZ. Of the RAFOS floats that were released at 1,800 dbar (in the upper plume of ISOW), 50% passed over the RR before reaching the CGFZ. Of those, 50% (or 25% of all floats) passed through the BFZ on their way to the Irminger Sea. Common to all RAFOS floats that entered BFZ is that they all passed through a narrow funnel-like bathymetric feature into the BFZ. In other words, if they reach the entrance to this bathymetric feature, they were likely to be shunted into the BFZ through the SC, as shown by those floats with well-resolved trajectories. It is expected that the float trajectories would be strongly constrained by bathymetry, given the quasi-barotropic character of the flow field (Koman et al., 2020), and the fact that the floats are drifting close to the bottom.

The two best-resolved trajectories through the BFZ showed a direct passage through the SC, in contrast to what was observed by daily profiling MARVOR floats, drifting at 1,950 m (Petit et al., 2022). The MARVOR floats traced out cyclonic circulation near the junction of the SC into the NC, and then westward into the Irminger Basin. We note here that the RAFOS floats were drifting at about 1,800 dbar, and that the MARVOR floats were caught in NC underneath the main ISOW outflow, in the part of the water column with weak westward velocities in the mean flow as measured by the moored current meters.

It remains to be determined what drives the variability through the BFZ, although we suspect that wind stress variations may be a factor given the interesting increase in transport reversals during the two winters observed. A link between wind stress and transport variability of the ERR Current (Koman et al., 2020) and ISOW transport at the CGFZ (Xu et al., 2018) were both evident. Studies of the time-evolution of water mass composition of the ERR, CGFZ, and BFZ moored instrument records, and further investigation of the annual cycle in ISOW transport, are planned for future work.

## Data Availability Statement

The BFZ mooring data may be found at <https://doi.org/10.26025/1912/69268> (Furey et al., 2024b). OSNAP RAFOS float, CTD, LADCP, and moored instrument data used in this study are available at <https://www.o-snap.org/data-access/>. Absolute dynamic topography are available at <https://cfs.climat.copernicus.eu/cdsapp#!/dataset/satellite-sea-level-global?tab=overview>. Argo Float data are available at <https://usgodae.org/argo/argo.html>. Multibeam data are available at <https://www.ncei.noaa.gov/maps/bathymetry/>.

## References

- Beaird, N. L., Rhines, P. B., & Eriksen, C. C. (2013). Overflow waters at the Iceland–Faroe Ridge observed in multiyear sea glider surveys. *Journal of Physical Oceanography*, 43(11), 2334–2351. <https://doi.org/10.1175/jpo-d-13-029.1>
- Bower, A., & Furey, H. (2017). Iceland-Scotland Overflow Water transport variability through the Charlie-Gibbs fracture zone and the impact of the North Atlantic current. *Journal of Geophysical Research – Oceans*, 122(9), 6989–7012. <https://doi.org/10.1002/2017JC012698>
- Bower, A., Ramsey, A., Furey, H., & Lozier, S. (2022). *What determines the pathways of Iceland-Scotland Overflow Water in the Eastern North Atlantic?* (Vol. 2022, p. OS25A-01). AGU Conference, December 2022.
- de Jong, M. F., de Steur, L., Fried, N., Bol, R., & Kritsotakis, K. (2020). Year-round measurements of the Irminger Current: Variability of a two-core current system observed in 2014–2016. *Journal of Geophysical Research: Oceans*, 125(10), e2020JC016193. <https://doi.org/10.1029/2020JC016193>
- Devana, M. S., Johns, W. E., Houk, A., & Zou, S. (2021). Rapid freshening of Iceland Scotland Overflow Water driven by entrainment of a major upper ocean salinity anomaly. *Geophysical Research Letters*, 48(22), e2021GL094396. <https://doi.org/10.1029/2021GL094396>
- Dickson, R. R., & Brown, J. (1994). The production of North Atlantic deep water: Sources, rates, and pathways. *Journal of Geophysical Research*, 99(C6), 12319–12341. <https://doi.org/10.1029/94JC00530>
- Fried, N., & de Jong, M. F. (2022). The role of the Irminger Current in the Irminger Sea northward transport variability. *Journal of Geophysical Research: Oceans*, 127(3), e2021JC018188. <https://doi.org/10.1029/2021JC018188>
- Fu, Y., Lozier, M. S., Bilo, T. C., Bower, A. S., Cunningham, S. A., Cyr, F., et al. (2023). Seasonality of the meridional overturning circulation in the subpolar North Atlantic. *Communications Earth & Environment*, 4(1), 181. <https://doi.org/10.1038/s43247-023-00848-9>
- Furey, H., Ramsey, A., & Bower, A. (2024a). *Bight Fracture Zone Experiment: Moored instrument data report, July 2015 - July 2017*. Woods Hole Oceanographic Institution. <https://doi.org/10.1575/1912/69315>

## Acknowledgments

We thank two anonymous reviewers for helpful comments and suggestions that greatly improved the final manuscript. We thank V. Thierry (IFREMER) for providing ship time during the RREX cruises in 2015 and 2017, and B. Hogue (WHOI) for deploying and recovering the BFZ moorings. We extend sincere thanks to W. Johns for valuable discussions regarding the equivalent width method for estimating ISOW transport from the mooring data, and X. Xu for valuable discussions about annual signals found in the HYCOM model. This work was funded by NSF Grants OCE-0926656, OCE-1756361, OCE-1756363, and OCE-1948505.



- Furey, H., Ramsey, A. L., & Bower, A. (2024b). Bight Fracture Zone Experiment moored instrument data [Dataset]. *Woods Hole Oceanographic Institution*. <https://doi.org/10.26025/1912/69268>
- Furey, H. H., & Ramsey, A. L. (2019). Overturning in the Subpolar North Atlantic Program (OSNAP) RAFOS float data collected June 2014 to January 2019 [Dataset]. *Woods Hole Oceanographic Institution*. <https://doi.org/10.26025/1912/24388>
- Hansen, B., & Østerhus, S. (2007). Faroe Bank Channel overflow 1995–2005. *Progress in Oceanography*, 75(4), 817–856. <https://doi.org/10.1016/j.pocean.2007.09.004>
- Hey, R., Martínez, F., Höskuldsson, Á., Eason, D. E., Sleeper, J., Thordarson, S., et al. (2016). Multibeam investigation of the active North Atlantic plate boundary reorganization tip. *Earth and Planetary Science Letters*, 435, 115–123. <https://doi.org/10.1016/j.epsl.2015.12.019>
- Holliday, N. P., Bersch, M., Berx, B., Chafik, L., Cunningham, S., Florindo-López, C., et al. (2020). Ocean circulation causes the largest freshening event for 120 years in eastern subpolar North Atlantic. *Nature Communications*, 11(1), 1–15. <https://doi.org/10.1038/s41467-020-14474-y>
- Johns, W. E., Devana, M., Houk, A., & Zou, S. (2021). Moored observations of the Iceland-Scotland Overflow plume along the eastern flank of the Reykjanes Ridge. *Journal of Geophysical Research: Oceans*, 126(8), e2021JC017524. <https://doi.org/10.1029/2021JC017524>
- Johns, W. E., Yao, F., Olson, D. B., Josey, S. A., Grist, J. P., & Smeed, D. A. (2003). Observations of seasonal exchange through the Straits of Hormuz and the inferred heat and freshwater budgets of the Persian Gulf. *Journal of Geophysical Research*, 108(C12). <https://doi.org/10.1029/2003JC001881>
- Kanzow, T., & Zenk, W. (2014). Structure and transport of the Iceland Scotland Overflow plume along the Reykjanes Ridge in the Iceland Basin. *Deep Sea Research Part I: Oceanographic Research Papers*, 86, 82–93. <https://doi.org/10.1016/j.dsr.2013.11.003>
- Koman, G., Johns, W. E., & Houk, A. (2020). Transport and evolution of the East Reykjanes Ridge Current. *Journal of Geophysical Research: Oceans*, 125(10), e2020JC016377. <https://doi.org/10.1029/2020JC016377>
- Lavender, K. L., Owens, W. B., & Davis, R. E. (2005). The mid-depth circulation of the subpolar North Atlantic Ocean as measured by subsurface floats. *Deep Sea Research Part I: Oceanographic Research Papers*, 52(5), 767–785. <https://doi.org/10.1016/j.dsr.2004.12.007>
- Li, F., Lozier, M. S., Bacon, S., Bower, A. S., Cunningham, S. A., De Jong, M. F., et al. (2021). Subpolar North Atlantic western boundary density anomalies and the Meridional Overturning Circulation. *Nature Communications*, 12(1), 3002. <https://doi.org/10.1038/s41467-021-23350-2>
- Lozier, M. S., Bower, A. S., Furey, H. H., Drouin, K. L., Xu, X., & Zou, S. (2022). Overflow water pathways in the North Atlantic. *Progress in Oceanography*, 208, 102874. <https://doi.org/10.1016/j.pocean.2022.102874>
- Lozier, M. S., Li, F., Bacon, S., Bahr, F., Bower, A., Cunningham, S., et al. (2018). A sea change in our view of overturning in the subpolar North Atlantic. *Science*, 363(6426), 516–521. <https://doi.org/10.1126/science.aau6592>
- Petit, T., Mercier, H., & Thierry, V. (2018). First direct estimates of volume and water mass transports across the Reykjanes Ridge. *Journal of Geophysical Research: Oceans*, 123(9), 6703–6719. <https://doi.org/10.1029/2018JC013999>
- Petit, T., Thierry, V., & Mercier, H. (2022). Deep through-flow in the Bight Fracture Zone. *Ocean Science*, 18(4), 1055–1071. <https://doi.org/10.5194/os-18-1055-2022>
- Ramsey, A., Furey, H., & Bower, A. (2020). *Overturning of the subpolar North Atlantic program (OSNAP): RAFOS float data report, June 2014–January 2019* (p. 511). Woods Hole Oceanographic Institution Tech. Rep. WHOI-2020-06. <https://doi.org/10.1575/1912/26515>
- Rosby, T., Dorson, D., & Fontaine, J. (1986). The RAFOS system. *Journal of Atmospheric and Oceanic Technology*, 3(4), 672–679. [https://doi.org/10.1175/1520-0426\(1986\)003<0672:TRS>2.0.CO;2](https://doi.org/10.1175/1520-0426(1986)003<0672:TRS>2.0.CO;2)
- Saunders, P. M. (1994). The flux of overflow water through the Charlie-Gibbs Fracture Zone. *Journal of Geophysical Research*, 99(C6), 12343–12355. <https://doi.org/10.1029/94JC00527>
- Taburet, G., Sanchez-Roman, A., Ballarotta, M., Pujol, M.-I., Legeais, J.-F., Fournier, F., et al. (2019). DUACS DT2018: 25 years of reprocessed sea level altimetry products. *Ocean Science*, 15(5), 1207–1224. <https://doi.org/10.5194/os-15-1207-2019>
- Van Aken, H. M., & Becker, G. (1996). Hydrography and through-flow in the north-eastern North Atlantic ocean: The NANSEN project. *Progress in Oceanography*, 38(4), 297–346. [https://doi.org/10.1016/s0079-6611\(97\)00005-0](https://doi.org/10.1016/s0079-6611(97)00005-0)
- Xu, X., Bower, A., Furey, H., & Chassignet, E. (2018). Variability of the Iceland-Scotland Overflow Water transport through the Charlie-Gibbs Fracture Zone: Results from an eddy simulation and observations. *Journal of Geophysical Research: Oceans*, 123(8), 5808–5823. <https://doi.org/10.1029/2018JC013895>
- Xu, X., Schmitz, W. J., Hurlburt, H. E., Hogan, P. J., & Chassignet, E. P. (2010). Transport of Nordic Seas Overflow Water into and within the Irminger Sea: An eddy-resolving simulation and observations. *Journal of Geophysical Research*, 115(C12). <https://doi.org/10.1029/2010JC006351>
- Zhao, J., Bower, A., Yang, J., Lin, X., & Zhou, C. (2018). Structure and formation of anticyclonic eddies in the Iceland Basin. *Journal of Geophysical Research: Oceans*, 123(8), 5341–5359. <https://doi.org/10.1029/2018jc013886>
- Zou, S., Bower, A., Furey, H., Lozier, S., & Xu, X. (2020). Redrawing the Iceland-Scotland Overflow Water pathways in the North Atlantic. *Nature Communications*, 11(1), 1–8. <https://doi.org/10.1038/s41467-020-15513-4>
- Zou, S., Bower, A. S., Lozier, M. S., & Furey, H. H. (2023). Deep ocean circulation in the subpolar North Atlantic observed by acoustically tracked floats. *Progress in Oceanography*, 211, 102975. <https://doi.org/10.1016/j.pocean.2023.102975>
- Zou, S., Lozier, S., Zenk, W., Bower, A., & Johns, W. (2017). Observed and modeled pathways of the Iceland Scotland Overflow Water in the Eastern North Atlantic. *Progress in Oceanography*, 159, 211–222. <https://doi.org/10.1016/j.pocean.2017.10.003>